CCFE
CULHAM CENTRE FOR FUSION ENERGY

UK Atomic Energy Authority

UKAEA-CCFE-PR(25)398

Haoran Ding, Jian Peng, Yiqiang Wang, Qiao Dai, Peishuang Zhou, David Knowles, Mahmoud Mostafavi

# Exploring stress states of notched small punch test specimens with different notch types

# Exploring stress states of notched small punch test specimens with different notch types

Haoran Ding, Jian Peng, Yiqiang Wang, Qiao Dai, Peishuang Zhou, David Knowles, Mahmoud Mostafavi

This is a preprint of a paper submitted for publication in Theoretical and Applied Fracture Mechanics

# Exploring stress states of notched small punch test specimens with different notch types

Haoran Ding[1], Jian Peng[1*], Yiqiang Wang[2], Qiao Dai[3], Peishuang Zhou[1], David Knowles[4], Mahmoud Mostafavi[4]

1 School of Mechanical Engineering and Rail Transit, Changzhou University, Changzhou 213164 China
2 United Kingdom Atomic Energy Authority, Culham Science Centre, Abingdon, Oxfordshire OX14 3DB, UK
3 School of Mechanical Engineering, Jiangsu University of Technology, Changzhou 213001, China
4 Department of Mechanical Engineering, University of Bristol, Bristol BS8 1TR, UK

**Abstract:** Notched small punch test (SPT) specimens with different types of notches have been adopted by many researchers to understand the fracture parameters of materials. However the specimen geometries have not been standardized and the effects of notch type on mechanical properties, failure mechanisms, and stress state of the tested materials need to be explored. The current work systematically studied the deformation behavior of a CuCrZr alloy using SPT specimens with side notch, groove notch, and circle notch, as well as different notch sizes using experimental and finite element simulation methods. Based on SPT load-displacement curves, the circle notch causes the greatest decrease in load-carrying capacity as it significantly affects the member stretching stage, and the differences between the side notch and groove notch are dependent on the notch size. Subsequently, the strain distributions around the centre line and on the notch arc are depicted to reveal the variation of strain distribution and failure mechanism with notch type and notch size. Moreover, quantitative characterizations of stress state parameters including stress triaxiality and Lode angle parameter at the notch tip and the specimen centre point are provided for the first time for notched SPT specimens with three notch types. This study comprehensively reveals the effects of notch type and size on the mechanical properties and stress state of SPT specimens, providing an essential reference for the utilization and standardization of notched SPT specimens.

**Keywords:** small punch test, notch type, stress state, mechanical property, failure mechanism

| Nomenclature | |
|---|---|
| $a$ | radius of circular bar notch (mm) |
| $a_1$ | side notch length dimension (mm) |
| $a_2$ | groove notch depth (mm) |
| $a_3$ | circle notch depth (mm) |
| $D$ | diameter of SPT specimen (mm) |
| $R$ | radius of notch or groove (mm) |
| $t$ | specimen thickness (mm) |
| $J_{IC}$ | fracture toughness (KJ/m$^2$) |

| | |
|---|---|
| $K_{IC}$ | plane strain fracture values (MPa· $m^{\frac{1}{2}}$) |
| $E$ | Young's modulus (GPa) |
| $\sigma_y$ | yield strength (MPa) |
| $\xi$ | normalized third deviatoric stress |
| $\eta$ | stress triaxiality |
| $\theta$ | Lode angle |
| $\bar{\theta}$ | Lode angle parameter |
| （$\sigma_1$，$\sigma_2$，$\sigma_3$） | three principal stresses (MPa) |
| （$p$，$q$，$r$） | three stress invariants (MPa) |
| $S$ | deviatoric stress tensor (MPa) |
| $I$ | unit tensor |
| $\sigma_m$ | hydrostatic stress (MPa) |
| $\bar{\sigma}$ | von mises equivalent stress (MPa) |
| $J_2$ | second invariants of the deviatoric stress tensor (MPa) |
| $J_3$ | third invariants of the deviatoric stress tensor (MPa) |
| | |
| *Abbreviations* | |
| SPT | small punch test |
| DBTT | ductile-brittle transition temperature |
| CTOD | crack tip opening displacement |
| CT | compact tension |
| LIM | laser-induced micromachining |
| PEEQ | equivalent plastic strain |

# 1 Introduction

Small punch test (SPT) is widely used to evaluate the mechanical properties of materials in nuclear power equipment, petrochemical equipment, additive manufacturing, etc., due to its micro-sampling advantage. It is particularly suitable for the damage evaluation of long-term serviced equipment materials. The SPT specimen is commonly used to evaluate mechanical properties such as tensile [1-3], creep [4, 5], fatigue [6, 7], and ductile-brittle transition temperature (DBTT) [8, 9]. Some researchers correlate the thickness reduction ratio of un-notched SPT specimens with fracture parameters at the moment of failure [10-12]. Since there is no pre-crack or crack-like notch on these un-notched SPT specimens, the stress state is significantly different from that of the classical fracture specimen, such as CT specimen. It lacks a fracture mechanics basis, correlating SPT results of un-notched specimens with fracture

toughness. Then, researchers attempted to use notched SPT specimens [13-15] to study fracture parameters. Due to the presence of notch, an initial stress concentration area is present on the SPT specimen, providing a similar stress state condition with the classical fracture specimens for evaluating fracture parameters. There are significant differences in notch types and sizes of notched SPT specimens used by researchers, as summarized in Table 1.

**Table 1 Summaries of different notched SPT specimens.**

| Notch Type | Researchers | Notch Size /mm | | Material | Research parameters |
|---|---|---|---|---|---|
| | | Width | Length | | |
| "U" shaped side notch | Alegre [17] | 0.15-0.20 | 4.0、4.5、5.0、5.5、6.0 | 15.5PH | J-integral、CTOD |
| | Lai [18] | 0.3 | 4.0、4.2、4.4、4.6、4.8、5.0、5.2、5.4 | P91 | $J_{IC}$ |
| | Shikalgar [16] | 0.20 | 4.0、4.5、5.0 | 20MnMoNi55、T91 | J-R curve、CTOD |
| | Dymáček [20] | 0.3 | 3.00、3.50、3.75、4.00、4.25、4.50 | Sanicro 25 | Creep failure time |
| "V" shaped side notch | Alegre [21] | — | 5.00 | AZ31-B Mg-alloy | Creep crack initiation time |
| | | Width | Depth | | |
| "U" shaped groove notch | Kumar [29] | 0.278 | 0.15 | T91、SS304LN | J-integral |
| | Álvarez [22] | 0.28 | 0.15 | S355、WM、H8、CrMoV | CTOD |
| | García [23] | 0.278 | 0.15 | CrMoV base metal、CrMoV weld metal | CTOD |
| | Martínez-Pañeda [24] | 0.278 | 0.15 | CrMoV1、CrMoV2 | CTOD |
| | Guan [25] | 0.25 | 0.20 | A350 | DBTT |
| | Matocha [26] | 0.25 | 0.20 | 14MoV6-3、P92、P22 | DBTT |
| | Wang [27] | 0.20 | 0.15、0.25 | 3Cr1MoV、2.25Cr1MoV、16MnR、A106 | DBTT |
| "V" shaped | Xu [15] | — | 0.50 | 16MnR | J-integral |

| | | | | | |
|---|---|---|---|---|---|
| groove notch | | | | | |
| | | Diameter | Depth | | |
| Circle notch | Turba [14] | 2.5 | 0.50 | P91 | DBTT |
| | Hurst [28] | 2.5 | 0.50 | P91 | $J_{IC}$、$K_{IC}$、DBTT |

"U" side notch is used to evaluate the fracture performance [16-18] and creep performance [19, 20] of metals. Alegre et al. [21] proposed to use a “V” side notched specimen as an alternative method for determining the creep crack initiation time when insufficient material is available for CT specimen. "U" groove notch is also used to evaluate fracture parameters [22-24] and ductile-brittle transition temperature [25-27]. Cuesta et al. [13] studied the influence of processing technology for "V" groove notch on SPT results, and found that laser-induced micromachining (LIM) is the most appropriate processing technology for "V" groove notch. Xu et al. [15] proposed using an equivalent Weibull stress method to determine the fracture toughness of materials by a “V” groove notched SPT specimen. In addition to side and groove notched specimens, Turba [14] proposed using circle notched SPT specimen to evaluate material fracture toughness. Since it was close to plane strain condition, this notched SPT specimen was used to evaluate $K_{IC}$ fracture toughness for sufficiently brittle materials. Later, Hurst [28] used circle notched specimen to test the fracture toughness of P91 steel and obtained similar results with Turba. Altought many researchers performed extensive studies on material fracture parameters using notched SPT specimens, notch type and size are not uniform. And there is no uniform notch type and size in existing SPT standards. Martínez-Paneda [23] found that the geometry of notch affected stress state and thus fracture behaviour.

The stress state is quantitatively represented by stress triaxiality and Lode angle parameter. Many studies revealed that, the stress state parameters affected the damage mechanics and failure mode. Lin [30] conducted a series of thermal tensile tests on circular bar specimens with different notch radii and found that fracture strain decreased with the increase of stress triaxiality. Kondori [31] and Li [32] proved that stress triaxiality significantly affected the growth of microvoids and ductile fracture toughness of alloys. Srivastave [33] and Zhu [34] observed that Lode angle parameter affected the development of void shape and subsequently controlled the damage evolution and fracture mechanisms. Ma [35] studied influence of initial porosity, stress triaxiality and Lode parameter on plastic deformation and ductile fracture, and found that stress triaxiality and Lode parameter affected the development of void volume fraction. These researches mainly used classical bar specimens, but the stress state of notched SPT specimen is not well understood.

Stress triaxiality and Lode angle parameter affect not only the damage evolution, but also the fracture mechanism. However, the stress state parameters of notched SPT specimens are not thoroughly revealed. Therefore, this paper studies mechanical properties, strain distribution and stress state of notched SPT specimens with different notch types and sizes, to fill the knowledge gaps regarding the stress state of notched SPT specimens.

## 2 Experimental and simulation of notched SPT specimens

### 2.1 Types of notched SPT specimens

The notch studied in this paper includes three types: side notch, groove notch and circle notch, as shown in Fig. 1. Due to the small size of notch, the manufacturing of U-shaped notch is easier than V-shaped notch. To ensure the reliability and repeatability of the experimental results, the "U" shape notch arc is used in this study. The notch radius of side notch and groove notch is 0.15mm. The circle notch is on a circle with a diameter of 2.5mm [14], and the radius of notch is 0.1mm.

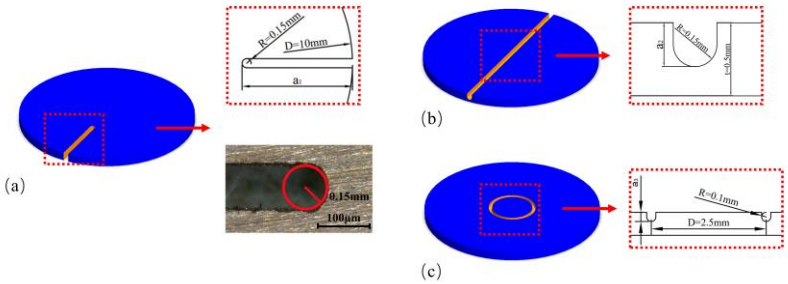


**Fig. 1 Three notch types: (a) side notch, (b) groove notch, (c) circle notch.**

The SPT specimens is with the diameter $D$ =10 mm and the thickness $t$=0.5 ± 0.005mm. For side notched SPT specimen, the notch length $a_1$ is expressed as the percentage of specimen diameter $D$. Seven levels of relative notch size are considered, and $a_1$ are (30%, 37.5%, 40%, 45%, 50%, 55%, 60%) × 10mm. For groove and circle notched SPT specimens, the notch depths $a_2$ and $a_3$ are expressed as the percentage of the specimen thickness $t$. Five levels of relative notch size are considered, while $a_2$ and $a_3$ are (30%, 40%, 50%, 60%, 70%) ×0.5mm.

### 2.2 Experiment of SPT specimen with side notch

The side notch is fabricated by wire cutting and with an accurate notch size, as shown in Fig. 1 (a). The relative sizes of groove and circle notch are quantified by the specimen thickness, which makes it challenging to guarantee processing accuracy. Therefore, both experiment and finite element simulation methods are used to study the side notched specimen, only the finite element simulation method is used to study the groove notched and circle notched specimen.

Fig. 2 shows SPT device, which includes upper die, lower die, ball and punch rod. The receiving hole of lower die has a diameter of 4mm with 0.2mm chamfer. The loading speed for all the tests is 0.1 mm/min, with displacement measured by an extensometer. The experimental proceduress meet the requirements of BS EN 10371-2021 Metallic materials small punch test method [36].

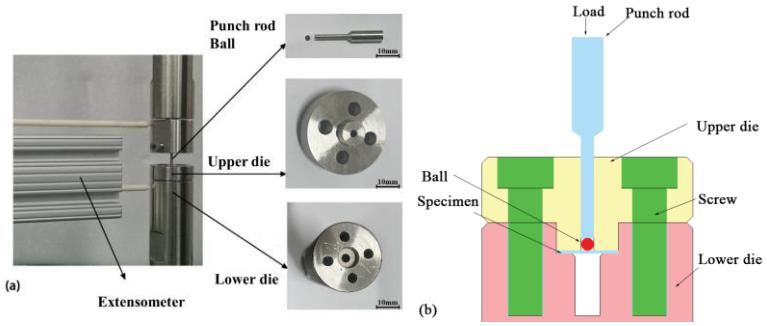


**Fig. 2 SPT device: (a) device diagram, (b) schematic diagram.**

CuCrZr copper alloy is used in the heat exchange tube of the plasma receiving structure in thermonuclear fusion equipment. According to the heat treatment of ITER-grade CuCrZr copper alloy, a solution annealing process is at 980°C for 30 minutes, followed by water quenching, and an aging treatment is performed at 460-500°C for 3 hours. The true stress-true strain curve of CuCrZr obtained by tensile test at room temperature is shown in Fig. 3, which is used in finite element simulation. The Young's modulus $E$ is 117 GPa and the yield strength $\sigma_y$ is 414MPa. The dimensions of tensile specimen meet the requirements of BS EN ISO 6892-1[37].

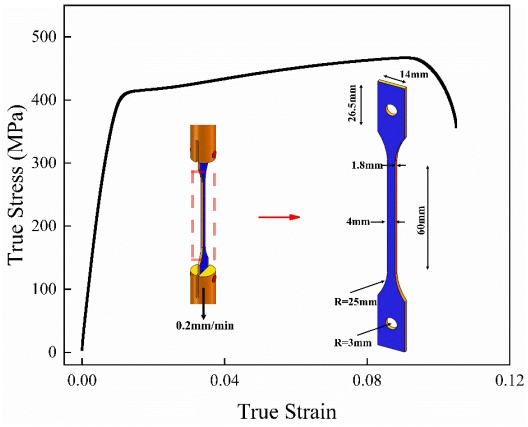


**Fig. 3 Characterization of CuCrZr Tensile Properties.**

### 2.3 Finite element simulation of notched SPT specimen

The un-notched and notched SPT specimens were simulated by ABAQUS. The simulation model is shown in Fig. 4(a), which simplifies the ball, the upper and lower dies as rigid bodies. The upper and lower dies are fixed, while a vertical displacement of 2mm is applied to the ball. The three-dimensional model of SPT specimen is meshing using eight-node elements (C3D8R) with reduced integration. The un-notched SPT specimen comprises 235,612 elements and 257,250 nodes, as shown in Fig. 4(b). The

meshing of side notched specimen is shown in Fig. 4(c). The finer mesh size with the element dimensions of 0.05mm×0.05mm×0.05mm is applied to the notch area and the contact area between punching ball and specimen to improve the simulation accuracy.

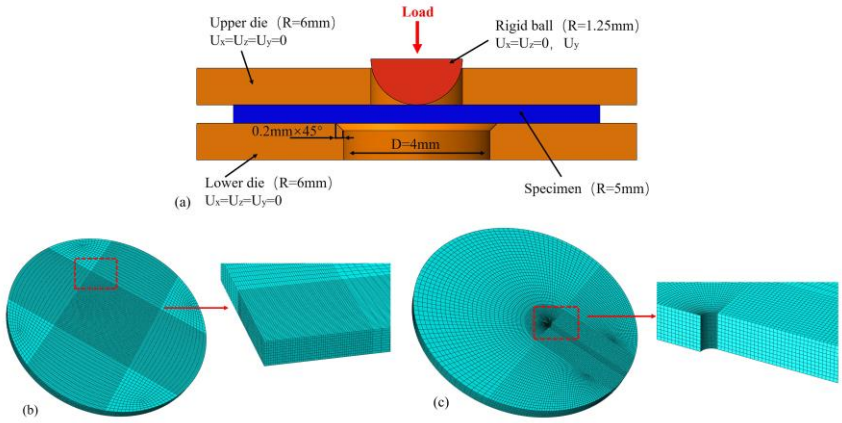


**Fig. 4 Finite element simulation of SPT: (a) simulation model, (b) meshing of un-notched specimen, (c) meshing of side notched specimen.**

In order to determine the friction coefficients, the simulation results with the friction coefficients ranging from 0.2 to 0.4 are compared with the experimental result for un-notched SPT specimen, in Fig. 5. The simulation error corresponding to the friction coefficient of 0.3 is the minimum. And the friction coefficient range between 0.2 and 0.3 is commonly used in references[38, 39]. Therefore, the friction coefficient of 0.3 is used in this study.

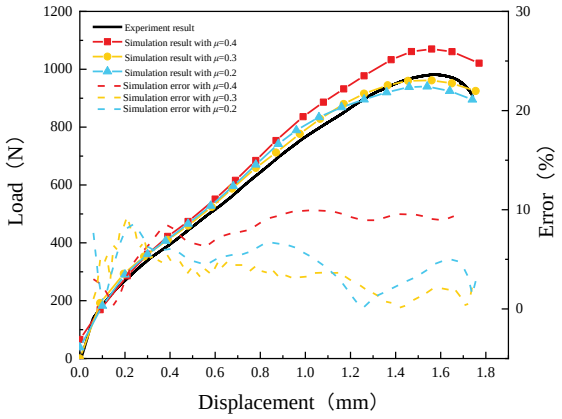


**Fig. 5 Comparison between SPT experimental results and simulation results with different friction coefficients.**

Fig. 6 compares the load-displacement curves between simulation and test. Results indicate good consistency between experimental and simulation curves for both un-notched and side notched specimens. And, some deviation appears at the failure stage, which is due to the lack of consideration for damage in finite element simulation.

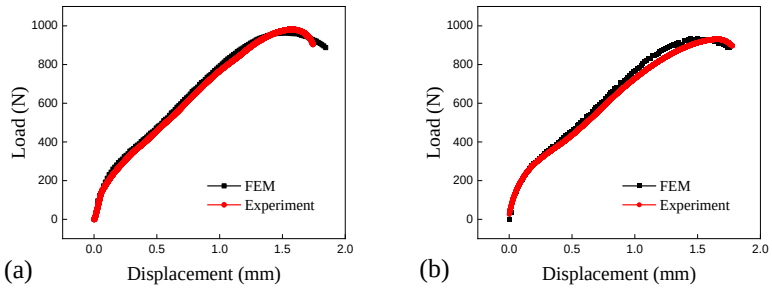


**Fig. 6 Comparison of SPT load-displacement curve between simulation and test: (a) un-notched specimen, (b) side notched specimen with the relative notch size of 40%.**

# 3 The influence of notch type on SPT load-displacement curve

## 3.1 The influence of side notch on SPT load-displacement curve

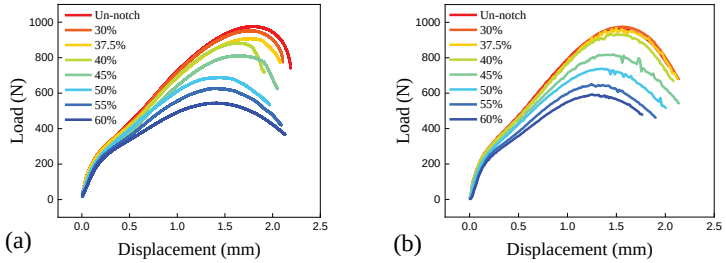


**Fig. 7 Load-displacement curves of side notched SPT specimen: (a) experimental results, (b) simulation results.**

Fig. 7 shows the load-displacement curves of side notched SPT specimens by experiment and simulation, respectively. The load-displacement curves of notched SPT specimens are similar in shape with that of un-notched specimen, but the slope and the mechanical parameters are affected by the side notch. It is worth noting that the influences at different relative side notch sizes are different.

(1) When the relative side notch size is 30%, since the notch is located outside the contact area between the ball and the specimen, the influence of the notch on the load-displacement curve is only reflected at the failure stage, and there is no obvious effect on other stages.

(2) When the relative side notch size is between 30% and 45%, the influence of the notch on the load-displacement curve extends to the membrane stretching stage, plastic instability stage and failure stage, and the maximum load of the side notched SPT specimen shows a significant decrease.

(3) When the relative side notch size is greater than or equal to 50%, the influence of side notch on the load-displacement curve covers all stages of the load-displacement curve. With the relative notch size increase, the load-displacement curve shows a significant downward trend, and the membrane stretching stage is significantly shortened.

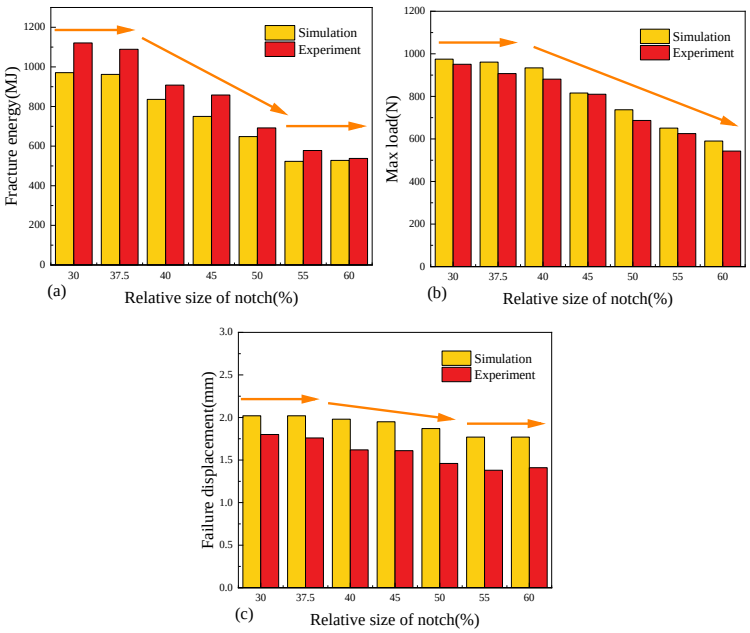


**Fig. 8 Variations of SPT mechanical parameters with the relative side notch size: (a) fracture energy, (b) maximum load, (c) failure displacement.**

Based on the SPT load-displacement curve, Fig. 8 shows variations of SPT strength parameter, displacement parameter and fracture energy with the relative side notch size. The SPT parameters of experiment and simulation show some differences for the failure displacement and fracture energy, but agree well for the maximum load. Moreover, the variation laws of SPT parameters with notch size also agree well for experimental and simulation results. When the relative side notch size is less than 37.5%, the parameters do not change significantly with the notch size, showing a plateau feature. When the relative notch size is between 40% and 55%, the mechanical, displacement and energy parameters show a linear decrease. After the relative notch size exceeds 55%, the fracture energy and failure displacement show a stable phenomenon, while the maximum load continues to decrease.

### 3.2 The influence of groove notch on SPT load-displacement curve

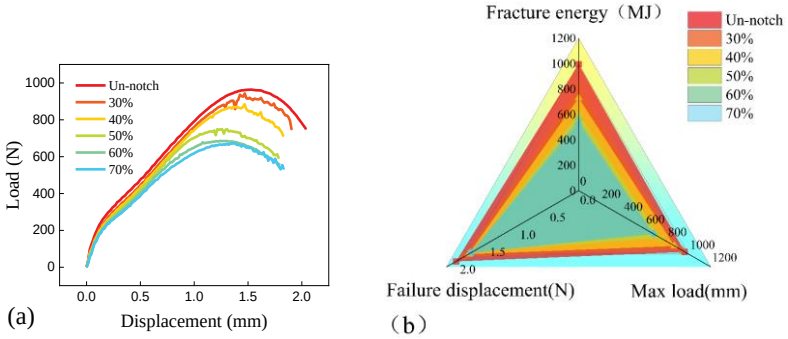


**Fig. 9 Load-displacement curves and mechanical parameters of groove notched SPT specimen: (a) load-displacement curve, (b) variations of mechanical parameters.**

Fig. 9 shows variations of the load-displacement curve and mechanical parameters with the relative notch size for the groove notched SPT specimens. In Fig. 9 (a), with the increase of the relative notch size, the load-displacement curve shows a decreasing trend in both load and displacement, and the influence of groove notch on the load-displacement curve covers the whole curve. When the relative notch size increases to 50%, the load-displacement curve drops sharply, which indicates that when the relative notch size is half of the specimen thickness, the failure mode of the groove notched SPT specimen may change. Fig. 9 (b) shows variations of SPT mechanical and energy parameters with the relative groove notch size. With the increase of the relative groove notch size, the failure displacement, fracture energy and maximum load gradually decrease. But the variation law is not linear, and when the relative groove notch depth is greater than 50%, the failure displacement tends to be stable.

### 3.3 The influence of circle notch on SPT load-displacement curve

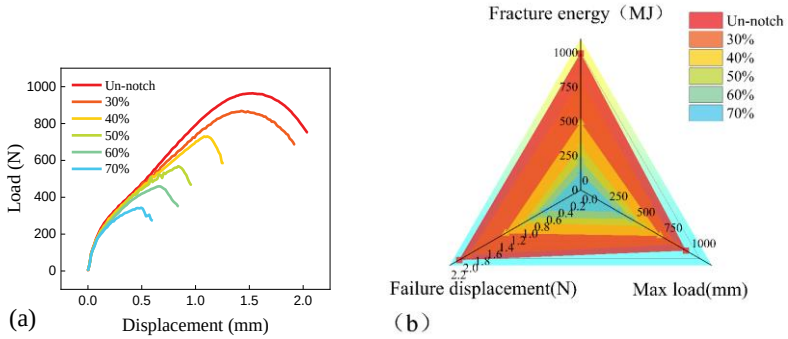


**Fig. 10 Load-displacement curves and mechanical parameters of circle notched SPT specimen: (a) load-displacement curve, (b) variations of mechanical parameters.**

Fig. 10 shows variations of the load-displacement curve and mechanical parameters

as a function of the relative notch size for the circle notched SPT specimens. In Fig. 10 (a), when the relative circle notch size is less than or equal to 30%, the load-displacement curve of the circle notched specimen contains five stages, which is similar to that of the un-notched specimen. With the relative circle notch size continues to increase, its membrane stretching stage becomes significantly narrower. When it increases to 50%, there is no membrane stretching stage, and it fractures once it reaches the plastic stage. Fig. 10 (b) shows variations of SPT mechanical and energy parameters with the relative circle notch size. With the increase of the relative circle notch size, the failure displacement, fracture energy and maximum load all show linearly decrease, reflecting the significant weakening of the circle notch on the load capacity of SPT specimen. The reason is that the circle notch destroys the membrane stretching stage, significantly decreasing its load capacity.

### 3.4 The influence of notch type on SPT mechanical parameters

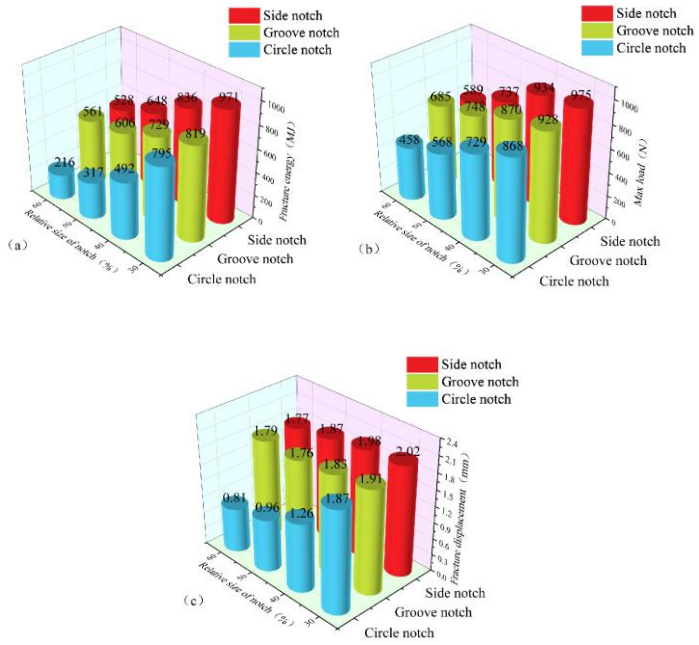


**Fig. 11 Variations of SPT mechanical parameters with the relative notch size for different notch type: (a) fracture energy, (b) maximum load, (c) fracture displacement.**

Fig. 11 compares variations of SPT mechanical parameters with notch size for three notch types. At the same notch size, all the fracture energy, maximum load and failure displacement of circle notched SPT specimen are lower than those of groove and side notch, and with the greatest decreasing rate. The maximum load shows a linear decrease law, while the fracture energy and failure displacement show a parabolic decrease law. The circle notch has the most significant weakening effect on the loading capacity, since

it destroys the membrane stretching stage of the SPT curve, and the effects of the other two notch types are limited on the local notch area. Comparing the side notch and the groove notch, when the relative notch size is less than 50%, the SPT mechanical parameters of groove notch, including maximum load, failure displacement and fracture energy, are lower than those of side notch. However, when the relative notch size is greater than 50%, the SPT mechanical parameters of groove notch are higher. Therefore, when the relative notch size is small, the groove notch has a greater weakening effect than the side notch, but the result is reversed when the relative notch size is large.

# 4 The influence of notch type on the strain distribution of SPT specimen

## 4.1 The influence of notch type and size on the strain distribution around the centre line of specimen

4.1.1 The influence of side notch on the strain distribution around the centre line of specimen

Fig. 12 shows the equivalent plastic strain (PEEQ) distribution curves around the centre line on the lower surface of the side notched SPT specimen, as well as the strain distribution contour maps on the centre cross-section. In Fig. 12, Stage 1, Stage 2, Stage 3, and Stage 4 represent the equivalent plastic strain distribution curves at the elastic bending stage, plastic bending stage, membrane stretching stage, and plastic instability stage.

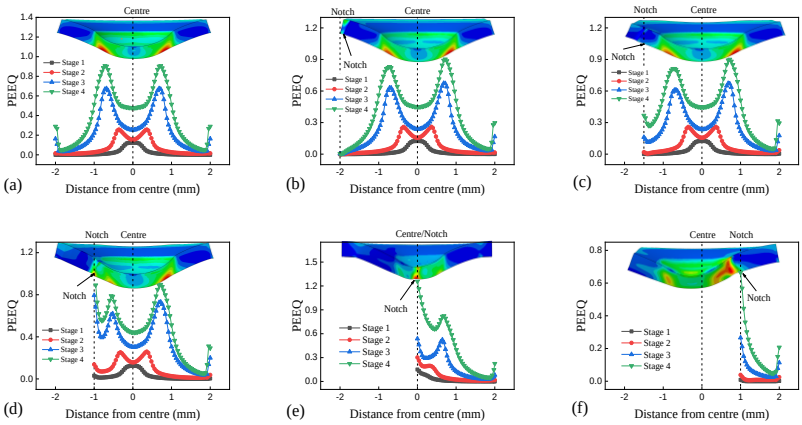


**Fig. 12 Equivalent plastic strain distribution curves of side notched SPT specimen: (a) un-notch, (b) 30%, (c) 37.5%, (d) 40%, (e) 50%, (f) 60%.**

For the un-notched specimen in Fig. 12 (a), in Stage 1 elastic bending stage, the maximum strain is located at the centre point of specimen. The contact between the punch ball and the specimen is the point contact in the elastic bending stage, and the

**Commented [WY1]:** Has this term been defined in this paper?

**Commented [WY2]:** A bit too late, but it would be nice to use the same Y axis.

plastic deformation only occurs in the centre and nearby area of the specimen. With the load increasing to Stage 2 plastic bending stage, the strain distribution curve shows an "M" shape, and the maximum strain is located at a ring with a certain distance from the specimen centre. Because the contact between the ball and the specimen changes from point contact to surface contact, the strain concentration area changes from the centre point to the circular ring. In Stage 4 plastic instability stage, the "M" shape strain concentration phenomenon is more significant, and a necking phenomenon of thickness reduction occurs at the strain concentration, which is about 0.75mm away from the specimen centre.

When the relative side notch size is less than or equal to 37.5% in Figs. 12 (b) and (c), the notch only affects the equivalent plastic strain distribution of the left half part of the specimen, and the strain concentration position does not change. In Fig. 12 (d), when the relative notch size increases to 40%, the strain concentration phenomenon at the notch significantly increases, and the strain concentration position changes from circular ring to notch tip. But the notch only affects one side of the specimen and has little effect on the other side. When the relative notch size reaches or exceeds 50% in Figs. 12 (e) and (f), the equivalent plastic strain at the notch position increases sharply, affecting the equivalent plastic strain distribution of the whole specimen, which is entirely different from that of the un-notched specimen.

In brief, for un-notched specimen, equivalent plastic strain distribution is the symmetrical "M" shape; when the relative notch size is less than 37.5%, side notch only affects one side of specimen, and strain concentration position is same as that of the un-notched specimen; when the relative notch size reaches 40%, strain concentration position changes from circular ring to notch tip; when the relative notch size is greater than or equal to 50%, side notch affects the whole specimen's strain distribution.

4.1.2 The influence of groove notch on the strain distribution around the centre line of specimen

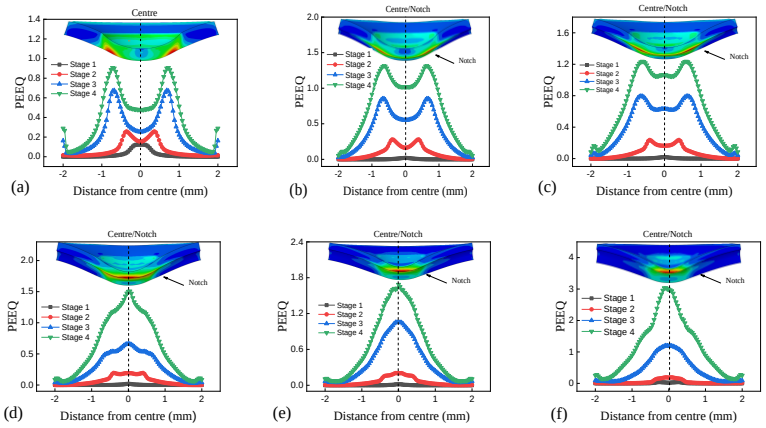


**Fig. 13 Equivalent plastic strain distribution curves of groove notched SPT specimen: (a) un-notch, (b) 30%, (c) 40%, (d) 50%, (e) 60%, (f) 70%.**

Fig. 13 shows the equivalent plastic strain distribution curves around the centre line on the lower surface of the groove notched SPT specimen, as well as the strain distribution contour maps on the centre cross-section. All groove notched SPT specimens have symmetrical strain distribution, but there are significant differences in strain distribution for different relative groove notch sizes. In Figs. 13 (b) and (c), when the relative notch size is 30%-40%, the strain distribution is still "M" shape, and the strain concentration point is still located at the circular ring with a certain distance from the specimen centre, but the strain in centre area increases. In Fig. 13 (d), when the relative notch size is 50%, the strain distribution curve changes from "M" shape to the inverted "V" shape, and the strain concentration point changes to the centre position of specimen. In Figs. 13 (e) and (f), the strain at the centre point increases sharply, and the slope of inverted "V" shape increases. Therefore, for the groove notched SPT specimen, when the relative notch size reaches 50%, it causes significant change in the strain distribution and the change of strain concentration position, which also causes the change of failure location of groove notched SPT specimen.

4.1.3 The influence of circle notch on the strain distribution around the centre line of specimen

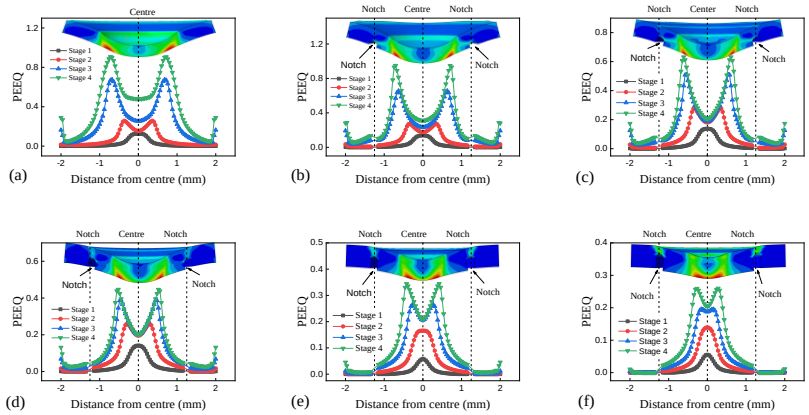


**Fig. 14 Equivalent plastic strain distribution curves of circle notched SPT specimen: (a) un-notch, (b) 30%, (c) 40%, (d) 50%, (e) 60%, (f) 70%.**

Fig. 14 shows the equivalent plastic strain distribution curves around the centre line on the lower surface of the circle notched SPT specimen, as well as the strain distribution contour maps on the centre cross-section. The strain distributions of circle notched SPT specimens are all symmetrical and with "M" shape. With the increase in the relative notch size, the strain concentration circular ring moves to the centre area, and the strain concentration character is gradually weak.

4.1.4 The influence of notch type on the strain distribution of SPT specimen

To directly reveal the effect of notch type on the strain distribution of SPT specimens, Fig. 15 shows the strain distributions of different notched SPT specimens at the Stage

3 membrane stretching stage, with the relative notch size range of 30%-60%.

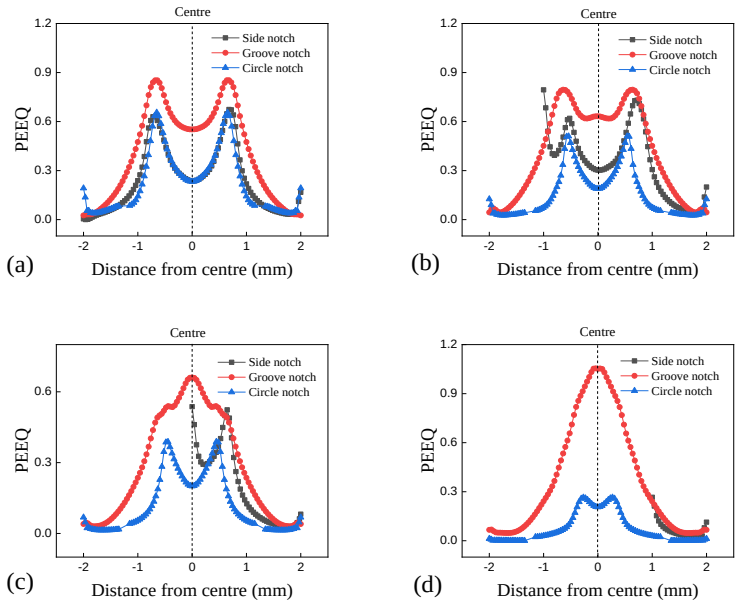


**Fig. 15 Effect of notch type on strain distribution curve: (a) 30%, (b) 40%, (c) 50%, (d) 60%.**

As shown in Fig. 15, when the relative notch size is 30%, the strain distribution laws of three types of notched specimens are similar, and those of side notch and circle notch are the same, while the strain value of groove notch is significantly higher than those of side notch and circle notch. With the increase of relative notch size, the strain concentration position of side notched SPT specimen changes to notch position, and that of groove notched SPT specimen changes to the specimen centre, while that of circle notched SPT specimen gathers to the specimen centre, but still has a certain distance from centre. Table 2 gives the strain concentration and strain distribution characters of different notch specimens, and the variation law is with the increase of relative notch size. For side notch, the strain concentration position changes from circular ring to notch position. For groove notch, the strain distribution changes from "M" shape to inverted "V" shape, and the strain concentration changes from circular ring to specimen centre. For circle notch, strain concentration area gathers to centre.

**Table 2 Comparison of strain distribution laws for different notch types.**

| Notch type | Strain concentration | Strain distribution |
|---|---|---|
| Side notch | Changes from circular ring to notch position | Changes from "M" shape to concentrated distribution at notch |
| Groove notch | Changes from circular ring to specimen centre | Changes from "M" shape to inverted "V" shape |
| Circle notch | Gathers from circular ring to specimen centre | "M" shape distribution, and gathers to specimen centre |

### 4.2 The influence of notch type and size on the strain distribution at the notch arc

4.2.1 The influence of side notch on the strain distribution at the notch arc

The strain distribution at the notch arc is essential in understanding the deformation behaviour and failure mode of notched SPT specimen. Fig. 16 shows the equivalent plastic strain distribution at the side notch arc, where the radius of the curve is the equivalent plastic strain, and the angle is the notch circumferential angle. Since the SPT curve is dominated by the membrane stretching stage, the strain distribution at the 50% of the peak load is selected, corresponding to the result at the membrane stretching stage.

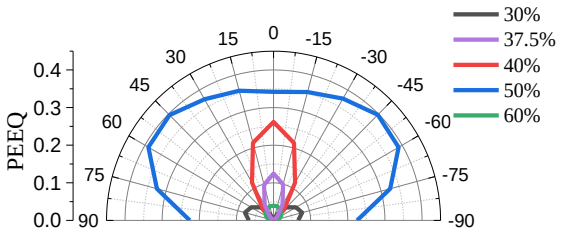


**Fig. 16 Equivalent plastic strain distribution curve at the notch arc for the side notch.**

As shown in Fig. 16, when the relative notch size is between 37.5% and 40%, the strain concentrates at the notch angle of 0° and decreases at both sides. When the relative notch size is lower than 30% and larger than 50%, the strain does not concentrate at the notch angle of 0°.

4.2.2 The influence of groove notch on the strain distribution at the notch arc

Fig. 17 shows the equivalent plastic strain distribution at the groove notch arc.

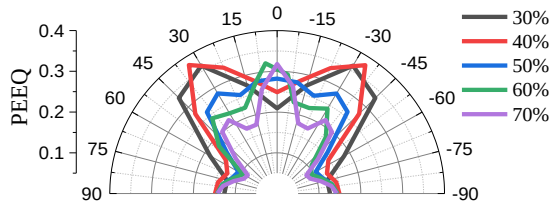


**Fig. 17 Equivalent plastic strain distribution curve at the notch arc for the groove notch.**

As shown in Fig. 17, when the relative notch size is 30%-40%, the maximum strain position is near the notch angle of ±40°, indicating a "Butterfly" shape. With the increasing of the relative notch size, the maximum strain position shifts to the notch angle of 0°, showing a strain concentration at the centre of the notch arc.

4.2.3 The influence of circle notch on the strain distribution at the notch arc

Fig. 18 shows the equivalent plastic strain distribution at the circle notch arc.

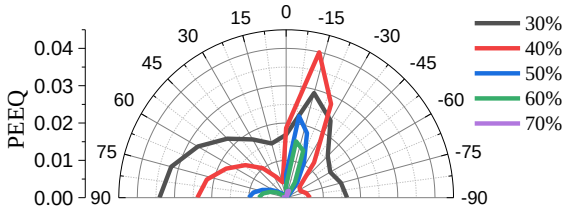


**Fig. 18 Equivalent plastic strain distribution curve at the notch arc for the circle notch**

As shown in Fig. 18, since the notch angle of -90° to 0° is close to the specimen centre, while that of 0° to 90°is close to specimen clamping side, the strain distribution at circle notch arc is asymmetric for all relative notch sizes, and strain concentration position is located at about -15° near notch centre. The strain distribution law at circle notch arc for different relative notch sizes is similar.

4.2.4 The influence of notch type on the strain distribution at the notch arc

To analyze the influence of notch type on strain distribution at notch arc more clearly, Fig. 19 compares the strain distribution curves at notch arc for different notch types.

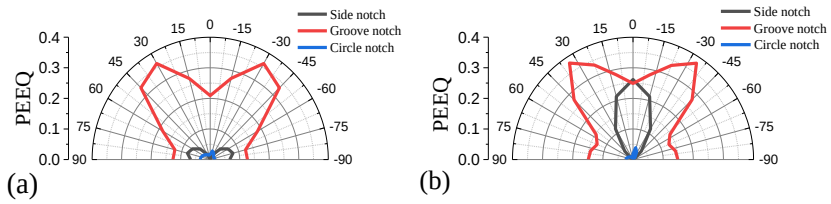

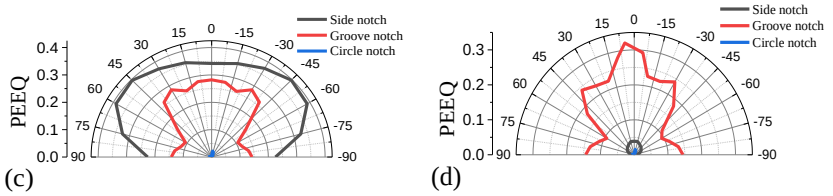


**Fig. 19 Effect of notch type on strain distribution curve at the notch arc: (a) 30%, (b) 40%, (c) 50%, (d) 60%.**

As shown in Fig. 19 (a), when the relative notch size is 30%, the strain at the notch arc does not show the strain concentration feature. When the relative notch size increases to 40% in Fig. 19 (b), only side notch shows the strain concentration feature at the notch angle of 0°. With the relative notch size increasing to 50%, the strain concentration of side notch disappears, and the strain at the groove notch arc gradually gathers to notch centre. When the relative notch size reaches 60%, the groove notch shows strain concentration feature at notch arc. For the circle notch, since one side of notch is close to specimen centre and the other is close to the clamping side. Therefore, the strain distributions at notch arc show asymmetric features for all relative notch sizes, and the strain concentration feature is not great.

### 4.3 The influence of side notch size on the failure mode of SPT specimen

Fig. 20 compares fracture morphologies of side notched SPT specimens with different notch sizes, and the strain cloud pattern diagram at the maximum load.

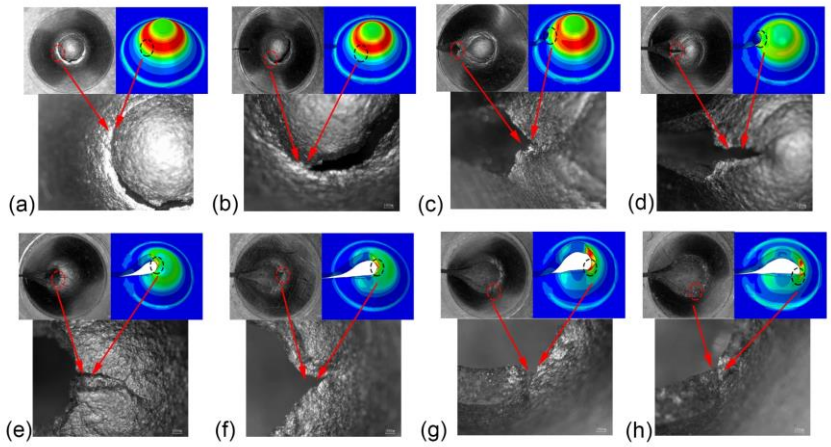


**Fig. 20 Fracture morphology of SPT specimen: (a) un-notch, (b) 30%, (c) 37.5%, (d) 40%, (e) 45%, (f) 50%, (g) 55%, (h) 60%.**

In Fig. 20 (a), the fracture area of un-notched SPT specimens shows a "cup-shaped bulge" feature. Under the loading action of punch ball, the local necking deformation ring appears, and at the maximum load, the main crack ring at the contact edge between ball and specimen causes the specimen fracture. When the relative side notch size is 30%

in Fig. 20 (b), the notch has no influence on failure location and fracture morphology.

With the relative size increasing to 37.5% in Fig. 20 (c), the fractured specimen still shows a "cup-shaped bulge" feature, but the failure location changes from the cup-shaped bulge edge to notch tip, and the crack-like failure morphology appears. When the relative side notch size is 40% in Fig. 20 (d), the "cup-shaped bulge" feature gradually weakens, and the crack initiation and growth at the notch tip is presented. When the relative side notch size is 45% in Fig. 20 (e), the "cup-shaped bulge" feature disappears, and the crack-like failure feature at the notch tip is still presented.

With the relative size increasing to 50% in Fig. 20 (f), when the notch is located at specimen centre, the failure location is at notch tip, but the crack-like failure feature weakens. In Figs. 20 (g) and (h), with the increase of the relative notch size, the failure location is no longer at the notch tip, but at the strain concentration position of the notch arc, and the failure mode is no longer the crack-like failure, but the toughness failure caused by large deformation.

It can be seen from the strain cloud pattern diagram shown in Fig. 20 that, when specimen is close to failure, the strain concentration position of finite element simulation matches with the fracture position in experiment. Therefore, the fracture of side notched SPT specimen is mainly due to the large plastic deformation and the strain concentration. It should be noted that, due to comprehensive effects of material and specimen structure, with the increase of side notch size, the failure mode of SPT specimen changes from ductile failure to crack fracture, and then to ductile failure. Table 3 summarizes the variations of failure location, cup convexity feature, crack feature and fracture mode with the notch size for the side notched SPT specimens.

**Table 3 Failure characteristics and failure modes of side notched SPT specimens.**

| Relative notch size | Failure location | Cup convexity feature | Crack feature | Fracture mode |
|---|---|---|---|---|
| None | Necking ring | Significant | No crack | Ductile fracture at necking ring |
| 30% | Necking ring | Significant | No crack | Ductile fracture at necking ring |
| 37.5% | Notch tip | Significant | Small crack, but un-propagation | Mixed fracture with crack and local large deformation |
| 40% | Notch tip | Insignificant | Crack propagation | Crack Growth |
| 45% | Notch tip | None | Crack propagation | Crack Growth |
| 50% | Notch tip | None | Small crack, but un-propagation | Mixed fracture with crack and local large deformation |
| 55% | Notch arc | None | No crack | Ductile fracture at notch arc |
| 60% | Notch arc | None | No crack | Ductile fracture at notch arc |

# 5 The influence of notch type on the stress state of SPT specimen

## 5.1 Quantitative representation of stress state

The stress state can be described by stress triaxiality and Lode angle parameters. The

concept of stress space is introduced to quantify the impact of stress state on material fracture behaviour. For isotropic materials, mechanical behaviour is independent of spatial direction, so that it can be represented by the three eigenvalues of the stress tensor, three principal stresses（$\sigma_1$，$\sigma_2$，$\sigma_3$）. The orthogonal principal stress space can be redefined in Lode coordinates, a cylindrical coordinate system with hydrostatic stress as its symmetry axis. Lode coordinates can be constructed from three stress invariants（$p$，$q$，$r$）, which are defined as:

$$p=-\sigma_m=-\frac{1}{3}tr(\sigma)=-\frac{1}{3}(\sigma_1+\sigma_2+\sigma_3) \tag{1}$$

$$q=\bar{\sigma}=\sqrt{\frac{3}{2}S:S}=\sqrt{\frac{1}{2}\left[(\sigma_1-\sigma_2)^2+(\sigma_2-\sigma_3)^2+(\sigma_3-\sigma_1)^2\right]}=\sqrt{3J_2} \tag{2}$$

$$r=\left[\frac{27}{2}\det(S)\right]^{1/3}=\left[\frac{27}{2}(\sigma_1-\sigma_m)(\sigma_2-\sigma_m)(\sigma_3-\sigma_m)\right]^{1/3}=\left[\frac{27}{2}J_3\right]^{1/3} \tag{3}$$

where $S$ is the deviatoric stress tensor, $S=\sigma-pI$, $I$ is the unit tensor, $\sigma$ is the stress tensor, $\sigma_m$ and $\bar{\sigma}$ are hydrostatic stress and Von Mises equivalent stress, $J_2$、$J_3$ are the second and the third invariants of the deviatoric stress tensor. When the specimen is in a compressive state, the parameter $p$ is positive, and when the specimen is in a tensile state, $\sigma_m$ is positive.

Stress triaxiality can reflect complex stress state, which significantly impacts the plastic deformation and fracture behaviour [16, 20]. It is an essential parameter for evaluating plastic constraint degree [40, 41] and is considered in plastic damage models[42]. It is defined as the ratio of hydrostatic stress to Von Mises stress:

$$\eta=\frac{\sigma_m}{\bar{\sigma}} \tag{4}$$

Experimental observations and numerical studies prove that, when establishing damage constitutive equations for ductile materials, the single stress triaxiality cannot fully reflect the impact of stress state on fracture behaviour [19, 21, 24]. The Lode angle parameter relating to the deviatoric stress state should be considered in conjunction with stress triaxiality for the stress state characterization. The Lode angle parameter $\bar{\theta}$ is defined as follows:

$$\xi=\left(\frac{r}{q}\right)^3=\cos(3\theta)=\frac{3\sqrt{3}}{2}\frac{J_3}{J_2^{3/2}}=\frac{27}{2}\frac{J_3}{q^3} \tag{5}$$

$$\bar{\theta}=1-\frac{6\theta}{\pi}=1-\frac{2}{\pi}\arccos\xi \tag{6}$$

The stress states of ten classic specimens are presented by stress triaxiality and Lode angle parameter, as listed in Table 4, where $R$ is radius of notch or groove, $a$ is radius of circular bar notch, and $t$ is thickness at grooving position on grooved plate [43].

**Commented [WY4R3]:** Check if the definition of Θ has been given ?

**Commented [WY3]:** The equation 6 should be 5, and make the equation 5 as 6?

**Table 4 Stress triaxiality and Lode angle parameter of ten classical specimens.**

| No. | Specimen type | Stress triaxiality | Lode angle parameter |
|---|---|---|---|
| 1 | Smooth round bars, tension | $1/3$ | 1 |
| 2 | Notched round bars, tension | $1/3+\sqrt{2}\ln(1+a/2R)$ | 1 |
| 3 | Plastic plane strain, tension | $\sqrt{3}/3$ | 0 |
| 4 | Flat grooved plates, tension | $\sqrt{3}/3\ [1+2\ln(1+t/4R)]$ | 0 |
| 5 | Torsion or shear | 0 | 0 |
| 6 | Cylinders, compression | $-1/3$ | -1 |
| 7 | Equi-biaxial plane stress, tension | $2/3$ | -1 |
| 8 | Equi-biaxial plane stress, compression | $-2/3$ | 1 |
| 9 | Plastic plane strain, compression | $-\sqrt{3}/3$ | 0 |
| 10 | Notched round bars, compression | $-[1/3+\sqrt{2}\ln(1+a/2R)]$ | -1 |

Special attention is given to the plane stress state under the condition of $\sigma_3$=0. Wierzbicki and Xue [44] proposed a correlation function of normalized third deviatoric stress $\xi$ and stress triaxiality $\eta$ (or Lode angle parameter $\bar{\theta}$):

$$\xi = \cos\left[\frac{\pi}{2}\left(1-\bar{\theta}\right)\right] = -\frac{27}{2}\eta\left(\eta^2-\frac{1}{3}\right) \tag{7}$$

The curve plot of above formula is shown in Fig. 21, where the stress states of ten classic specimens in Table 4 are marked with red circles [43].

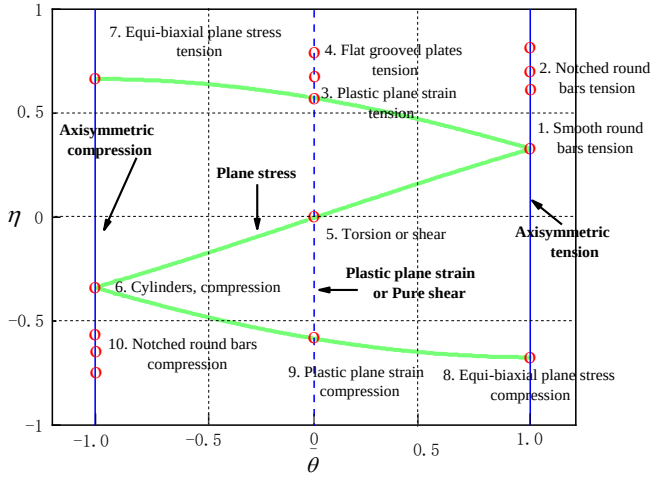


**Fig. 21 The representation of stress triaxiality and Lode angle parameter at initial state** [43]

## 5.2 The influence of notch type and size on the stress state around the centre line of specimen

For classical specimens, the stress triaxiality and Lode angle parameters are summarized in Fig. 21 and Table 4. However, the stress state of SPT specimens with different notch types is not well understood and revealed. Therefore, this paper aims to study the influence of notch type and size on the stress state of SPT specimens.

### 5.2.1 The influence of side notch on the stress state around the centre line of specimen

Fig. 22 shows the stress triaxiality distribution curves on the centre line of the lower surface for the side notched SPT specimens and the cloud pattern of stress triaxiality on the centre section.

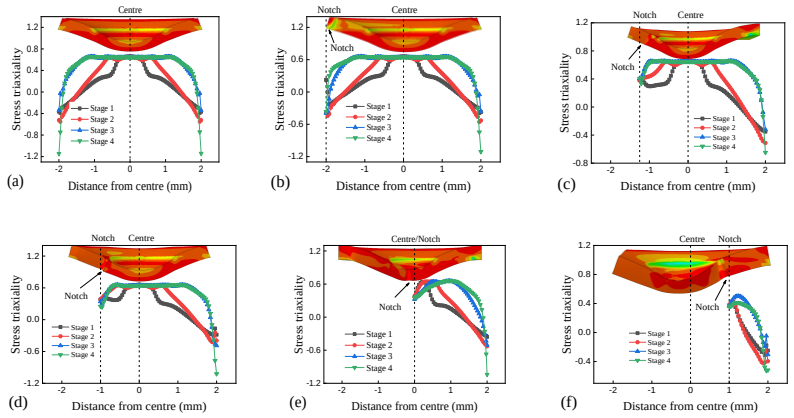


**Fig. 22 Stress triaxiality distribution curves of side notched SPT specimen: (a) un-notch, (b)30%, (c)37.5%, (d)40%, (e)50%, (f)60%.**

For un-notched SPT specimens in Fig. 22(a), at the elastic stage, the stress triaxiality within ±0.5mm range of the centre on the specimen lower surface is close to 0.65, and at the elastic-plastic stage, the flat region of stress triaxiality expands, while at the membrane stretching stage and plastic instability stage, the flat region expands to ±1.2mm. The stress triaxiality of 0.65 indicates that the lower surface of the specimen is in a biaxial tensile state. At the chamfer of the lower die (±2mm distance from the centre), the stress triaxiality decreases rapidly and becomes negative, which is due to the compressive state at the contact surface between SPT specimen and the chamfer of the lower die. When the relative side notch size is small in Fig. 22 (b), the notch is far from the specimen centre, so it has little effect on the stress triaxiality on the centre line of the lower surface. But, the stress triaxiality concentrates at the notch tip. As the relative notch size increases in Figs. 22 (c) and (d), the side notch only affects the stress triaxiality distribution in the left half part of specimen, and has little effect in middle point and right side. When the notch expands to centre point of specimen in Fig. 22(e), the stress triaxiality at the centre point decreases, and the notch has significant impact on stress triaxiality distribution of the whole specimen. When the relative notch size is

larger than 0.5 in Fig. 22(f), the biaxial tensile state with stress triaxiality of 0.65 no longer appears on the lower surface of specimen.

For un-notched SPT specimens, stress triaxiality is symmetrically distributed, and there is a central biaxial tensile region with the stress triaxiality of 0.65 on lower surface. When the relative notch size is 30%, the side notch only affects stress triaxiality at the notch tip. With the further increasing of notch size, the central biaxial tensile region narrows, and when the relative notch size is greater than 50%, the central biaxial tensile region disappears.

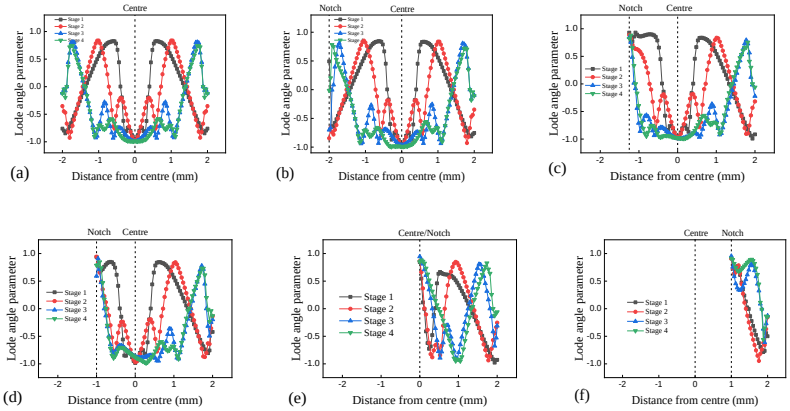


**Fig. 23 Lode angle parameter distribution curves of side notched SPT specimen: (a) un-notch, (b)30%, (c)37.5%, (d)40%, (e)50%, (f)60%.**

Fig. 23 shows distribution curves of Lode angle parameter on the centre line of the lower surface for side notched SPT specimens. In Fig. 23(a), for un-notched SPT specimen, Lode angle parameter on the central region of the lower surface is relatively stable and close to -1. Combined with the stress triaxiality of 0.65 in Fig. 22 and Lode angle parameter -1 in Fig. 23, there is a biaxial tensile region on lower surface for un-notched SPT specimens. In Fig. 23(b), when the notch is small and far from specimen centre, the side notch has no effect on Lode angle parameter on the centre area, and it only affects the Lode angle parameter distribution at notch tip. In Figs. 23(c) and (d), when the relative notch size increases to 40%, Lode angle parameter at notch is close to 1, but the notch only affects Lode angle parameter distribution in left half part of specimen and has no obvious effect on distribution of Lode angle parameter in middle point area and the right half part. In Figs. 23(e) and (f), as the relative notch size further increases, when the notch is located at or passes through the centre point of the specimen, the side notch significantly impacts the Lode angle parameter distribution on the centre line of the specimen. And the region with a biaxial tensile stress state disappears.

For un-notched SPT specimen, the Lode angle parameter is symmetrically distributed, at the central area it is relatively stable and close to -1. When the relative size is less than 40%, the notch only affects the Lode angle parameter distribution on the half side,

and the central area is still in a biaxial tensile stress state. As the relative notch size continues to increase, the biaxial tensile stress state disappears.

5.2.2 The influence of groove notch on the stress state around the centre line of specimen

Fig. 24 shows the stress triaxiality distribution curves on the centre line of the lower surface for groove notched SPT specimens and cloud pattern of stress triaxiality on centre section.

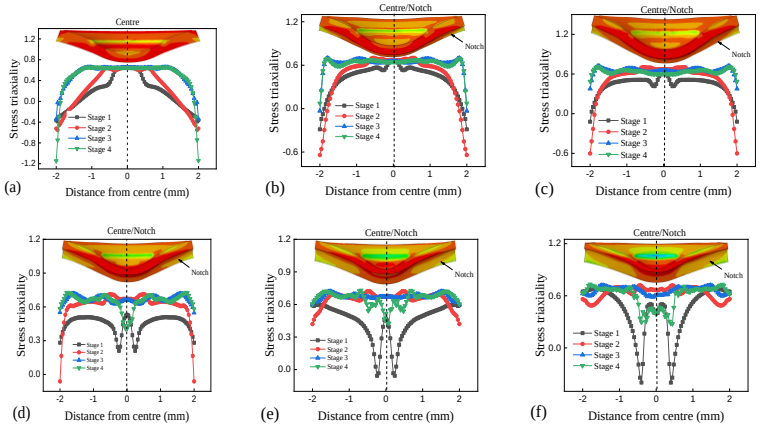


**Fig. 24 Stress triaxiality distribution curves of groove notched SPT specimen: (a) un-notch, (b) 30%, (c) 40%, (d) 50%, (e) 60%, (f) 70%.**

In Fig. 24, the groove notch significantly affects the stress triaxiality distribution in any notch size. In Figs. 24(b) and (c), when the relative groove notch size is 30%-40%, the stress triaxiality in central line of the lower surface is close to 0.65, similar to un-notched specimen, but in the distance range from ±1mm to ±2mm, it is significantly higher than that of un-notched SPT specimen. In Fig. 24(d), when the relative notch size is 50%, the stress triaxiality in the central area decreases and fluctuates in the elastic stage, while at the plastic stage, the stress triaxiality is around 0.6 in any distance. In Figs. 24(e) and (f), with the relative notch size further increasing, the fluctuation degree of stress triaxiality in central area increases, and the stress triaxiality continues to decrease at the elastic stage.

Therefore, when the relative groove notch size is lower than or equal to 40%, the stress triaxiality in the central area of the lower surface is close to 0.65, similar to stress triaxiality of biaxial tensile state, but when the relative notch size is greater than or equal to 50%, the stress triaxiality significantly decreases at the elastic stage, and the stress state in central area on lower surface of SPT specimens deviates from biaxial tensile state.

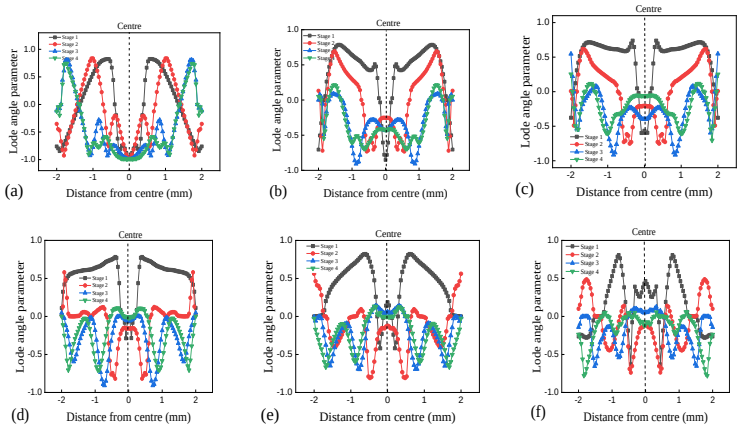


**Fig. 25 Lode angle parameters distribution curves of groove notched SPT specimen: (a) un-notch, (b) 30%, (c) 40%, (d) 50%, (e) 60%, (f) 70%.**

Fig. 25 shows distribution curves of Lode angle parameter on the centre line of the lower surface for groove notched SPT specimens. The groove notch significantly affects overall distribution of Lode angle parameter in any notch size. As the relative groove notch size increasing, Lode angle parameter in central area on lower surface increases. When the relative groove notch size reaches 60%, Lode angle parameter at the central point changes from negative value to positive value at the elastic stage. Therefore, as the relative groove notch size increasing, Lode angle parameter at the central area of SPT specimen is deviating from biaxial tensile state. At the same time, from fluctuation phenomenon in curves it can be seen that Lode angle parameters at different positions in SPT specimens change significantly. Presence of groove notch will make distribution of Lode angle parameters more complex.

5.2.3 The influence of circle notch on the stress state around the centre line of specimen

Fig. 26 shows the stress triaxiality distribution curves on the centre line of the lower surface for the circle notched SPT specimens and the cloud pattern of stress triaxiality on centre section.

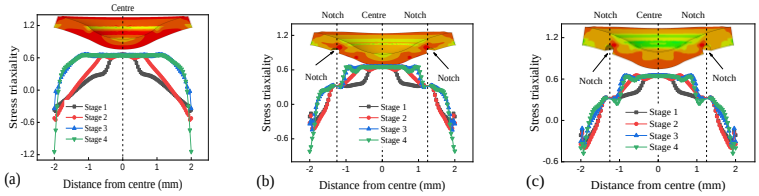

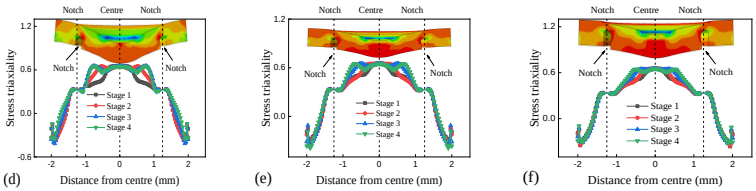


**Fig. 26 Stress triaxiality distribution curves of circle notched SPT specimen: (a) un-notch, (b) 30%, (c) 40%, (d) 50%, (e) 60%, (f) 70%.**

In Fig. 26, the circle notch affects not only the stress triaxiality distribution in the notch location, but also the central flat range of stress triaxiality in the central area. With the relative circle notch size increasing, the biaxial tensile region with the stress triaxiality of 0.65 at the centre of the lower surface is narrowing, but this region always exists. At the circle notch location, the stress triaxiality is close to 0.33, and the stress triaxiality in this region does not change with the notch size. Furthermore, when the relative circle notch size is larger than 50%, the stress triaxiality distribution curves at different stages coincide, indicating that when the relative circle notch size is large enough, the stress triaxiality of the circle notch does not change with the increase of loading displacement.

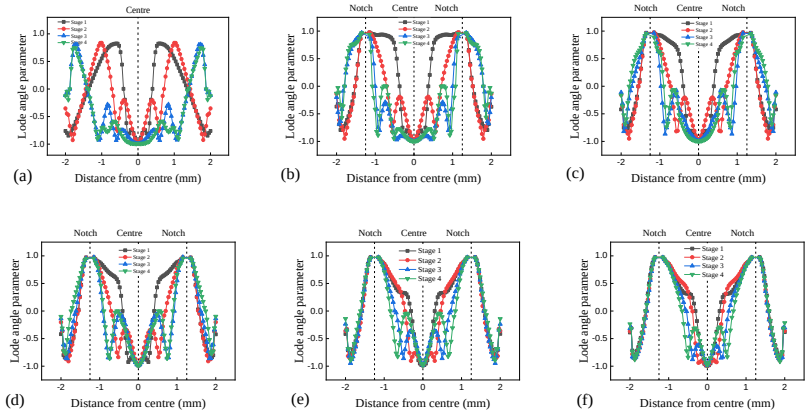


**Fig. 27 Lode angle parameter distribution curves of circle notched SPT specimen: (a) un-notch, (b) 30%, (c) 40%, (d) 50%, (e) 60%, (f) 70%.**

Fig. 27 shows distribution curves of Lode angle parameter on the centre line of the lower surface for circle notched SPT specimens. In central area on the lower surface for circle notch specimen, the Lode angle parameter is -1, and the stress triaxiality is 0.65, so the central area on lower surface for circle notch specimen is in biaxial tensile stress state. With the relative notch size increasing, the central biaxial tensile region is narrowing. At the circle notch location, Lode angle parameter is close to 1 and stress triaxiality is close to 0.33, so the stress state at notch location is close to axisymmetric

tensile state. When the relative circle notch size is greater than 50%, the distribution curves of Lode angle parameter at different stages coincide, so the loading displacement has no obvious effect on the Lode angle parameter distribution.

### 5.3 The influence of notch type and size on the stress state at the notch arc

5.3.1 The influence of side notch on the stress state at the notch arc

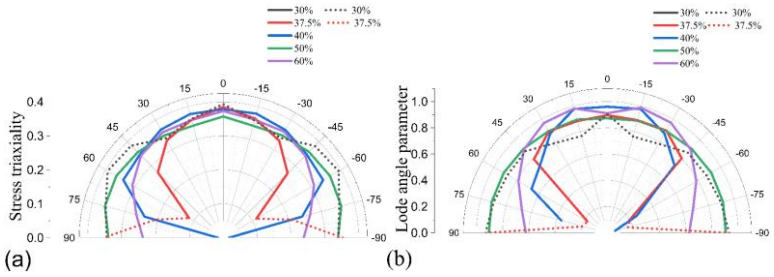


**Fig. 28 Stress state parameters distribution at the notch arc for the side notch: (a) Stress triaxiality distribution; (b) Lode angle parameter distribution.**

Fig. 28 shows the stress triaxiality and Lode angle parameter distributions on the side notch arc at the membrane stretching stage (i.e., 50% peak load), where negative values are taken as absolute ones and represented by dashed lines. When the relative notch size is 30%, the stress triaxiality values at the notch arc are all negative, while the Lode angle parameter at the notch arc is negative and uniformly distributed. When the relative notch size increases to 37.5%, both stress triaxiality and Lode angle parameter change from negative to positive within the notch angle range of ±60°. With the relative notch size further increasing, both stress triaxiality and Lode angle parameter values at the notch arc become positive, with stress triaxiality being almost independent of notch size within the range from 0.3 to 0.4, and Lode angle parameter being between 0.7-1

For side notched specimen, as the relative notch size increases, both stress triaxiality and Lode angle parameter change from negative to positive on notch arc, and the transition relative notch size is 37.5%. At smaller relative side notch sizes, the stress state parameters (stress triaxiality, Lode angle parameter) at notch arc are approximately (-0.36, -0.66), while at larger notch sizes, stress state parameters at notch arc are approximately (0.36, 0.66). The absolute values of both stress triaxiality and Lode angle parameter on the notch arc are independent of side notch size.

5.3.2 The influence of groove notch on the stress state at the notch arc

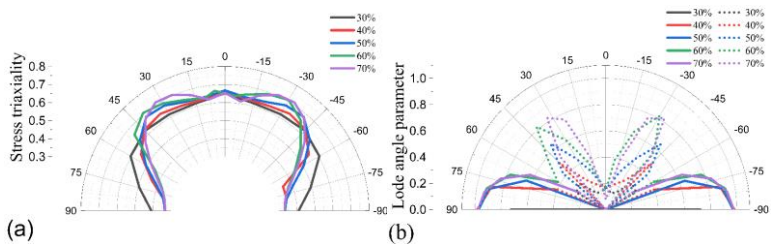

**Fig. 29 Stress state parameters distribution at the notch arc for the groove notch: (a) Stress triaxiality distribution; (b) Lode angle parameter distribution.**

Fig. 29 shows the stress triaxiality and Lode angle parameter distributions on the groove notch arc at the membrane stretching stage (i.e., 50% peak load), where negative values are taken as absolute ones and represented by dashed lines. In Fig. 29 (a), the stress triaxiality is symmetrical and around 0.6, and they almost coincide for different groove notch sizes, indicating that the groove notched SPT specimen is in a tensile state at the notch arc and the relative notch size has little effect on stress triaxiality at the notch arc. In Fig. 29 (b), the distributions of Lode angle parameter are not uniform on the groove notch arc, with negative values in the notch angle range of ±60°and positive values in the range of ±60° to ±90°. The distributions of Lode angle parameter are almost the same for different relative groove notch sizes, indicating that the relative groove notch size has no effect on Lode angle parameter distribution on the notch arc.

For groove notched specimen, stress triaxiality and Lode angle parameter on notch arc are independent on the notch size, and stress triaxiality is uniformly distributed around 0.6, while Lode angle parameter is negative in centre of the notch arc and positive in both sides of the notch arc.

5.3.3 The influence of circle notch on the stress state at the notch arc

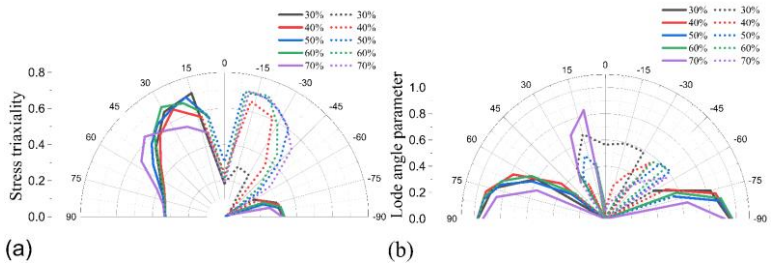


**Fig. 30 Stress state parameters distribution at the notch arc for the circle notch: (a) Stress triaxiality distribution; (b) Lode angle parameter distribution.**

Fig. 30 shows the stress triaxiality and Lode angle parameter distributions on the circle notch arc at the membrane stretching stage (i.e., 50% peak load), where negative values are taken as absolute ones and represented by dashed lines. In Fig. 30 (a), the stress triaxiality distribution is half positive and half negative on the notch arc of the circle notch specimens, with obvious asymmetry in the stress state on both sides of the notch arc. The stress triaxiality on the notch arc coincides for different notch sizes, indicating that the notch size has no effect on the stress triaxiality distribution on the notch arc. In Fig. 30 (b), Lode angle parameter is negative in centre of the notch arc and positive in both sides of the notch arc for circle notches, with similar distributions for different notch sizes, indicating that the relative size of the circle notch has no significant effect on Lode angle parameter distribution on the notch arc.

For the circle notched specimen, the stress triaxiality and Lode angle parameter at notch arc are not affected by the relative notch size. Stress triaxiality presents a

characteristic of positive values on one side and negative values on the other side, while Lode angle parameter is negative in centre of the notch arc and positive in both sides of the notch arc.

### 5.4 Stress state characterization of notched SPT specimen

The above analysis shows that variations of load-displacement curve, strain concentration feature and stress state with notch size are significantly different for different notch types. To characterize mechanical response, strain feature and stress state of notched SPT specimen, Table 5 summarizes variation rules of various characteristic parameters for different notch types. The characterization in the table represents the variation rule with the relative notch size increasing.

**Table 5 Comparison of SPT characteristic parameters for different notch types, with the relative notch size increasing.**

| SPT characteristic parameters | | Notch type | | |
|---|---|---|---|---|
| | | **Side notch** | **Groove notch** | **Circle notch** |
| **Load-displacement curve** | **Load-displacement curve** | Slope decreases, peak load decreases | Slope un-changes, peak load decreases | Membrane stretching stage shortens |
| | **Maximum load** | Gradually decreases | Gradually decreases | Rapidly decreases |
| | **Failure displacement** | Gradually decreases | Decreases then stabilizes | Rapidly decreases |
| | **Fracture energy** | Gradually decreases | Decreases then stabilizes | Rapidly decreases |
| **Strain distribution** | **On centre line** | Strain concentration changes from ring to notch | Strain concentration changes from ring to centre point | Strain concentration gathers to centre area |
| | **On notch arc** | Symmetric distribution and notch size dependent | "Butterfly" distribution and notch size independent | Asymmetric distribution and notch size independent |
| **Stress triaxiality** | **On centre line** | Affect limits at notch location | Affect covers the whole specimen | Affect limits at notch location |
| | **On notch arc** | Symmetrical distribution and changes from negative to positive | Symmetrical distribution and notch size independent | Asymmetrical distribution and notch size independent |
| **Lode angle parameter** | **On centre line** | Affect limits at notch location | Affect covers the whole specimen | Affect limits at notch location |
| | **On notch arc** | Symmetrical distribution and changes from negative to positive | Symmetrical distribution and notch size independent | Asymmetrical distribution and notch size independent |

Table 5 provides a comprehensive understanding of mechanical parameters, energy parameter, strain concentration characteristics, and stress state parameters for SPT

specimens with different notch types. But, the stress state of notched SPT specimens is still not quantitatively characterized. Quantitative characterization of stress state for different notched SPT specimens is currently a knowledge gap in small punch test research. Table 6 gives the quantitative characterization of stress state for different notched SPT specimens, and the relative notch size of 40% and 50% is considered, while the stress state of both the centre point on the lower surface and notch tip is given.

**Table 6 Quantitative characterization of stress state for SPT specimens with different notch types.**

| Stress state parameters | | Side notch | | Groove notch | | Circle notch | |
|---|---|---|---|---|---|---|---|
| | | 40% | 50% | 40% | 50% | 40% | 50% |
| **Notch tip** | **Stress triaxiality** | 0.3 | 0.3 | 0.65 | 0.65 | -0.25 | -0.25 |
| | **Lode angle parameter** | 1 | 1 | -0.4 | 0 | 0 | 0 |
| | **Stress state** | Axisymmetric tensile | Axisymmetric tensile | Between biaxial tensile and plane strain tensile | plane strain tensile | Between plane strain compression and shear | Between plane strain compression and shear |
| **Centre point on the lower surface** | **Stress triaxiality** | 0.65 | 0.3 | 0.65 | 0.65 | 0.65 | 0.65 |
| | **Lode angle parameter** | -1 | 1 | -0.4 | 0 | -1 | -1 |
| | **Stress state** | Biaxial tensile | Axisymmetric tensile | Between biaxial tensile and plane strain tensile | plane strain tensile | Biaxial tensile | Biaxial tensile |

The stress triaxiality and Lode angle parameter for notched SPT specimen at 40% and 50% notch size are shown in Fig. 31, which is added in the representation plot of stress triaxiality and Lode angle parameter for classical specimens.

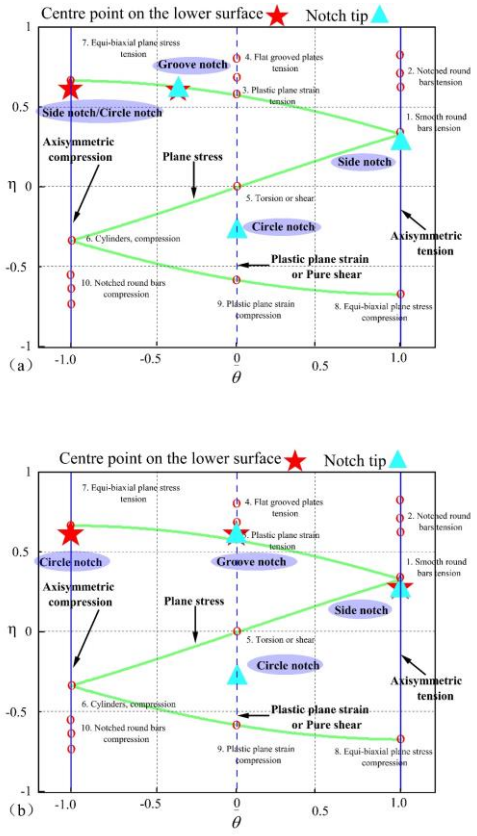


**Fig. 31 The representation of stress triaxiality and Lode angle parameter for different notched SPT specimens:(a) 40%, (b) 50%.**

From Table 6 and Fig. 31, it can be found that:

(1) Side notched SPT specimen produces different stress states at notch tip and at centre point on lower surface. At centre point, it is with the biaxial tensile state, while at notch tip, it is close to the axisymmetric tensile state. The stress state at the notch tip is beneficial for the crack initiation and propagation. Therefore, side notched SPT specimens are suitable for fracture toughness testing to explore the fracture parameters.

(2) Groove notched specimen produces the same stress state at notch tip and at centre point on lower surface, which is between biaxial tensile and plane strain tensile states. This stress state is better suitable for bending strength testing, rather than the fracture toughness testing.

(3) Circle notched specimen produces different stress states at notch tip and at centre point on lower surface. At centre point, it is in the biaxial tensile state, while at notch tip it is between plane strain compression and shear state. This stress state makes circle notched specimens better suitable for shear testing, rather than the fracture toughness

testing.

(4) For side notched specimen, as the relative notch size increases, the stress triaxiality and Lode angle parameter at notch tip are not changed, and the relative length of the side notched specimen should preferably not exceed 50%, since sufficient crack propagation length can be obtained. For groove notched specimen, as the relative notch size increases, the distribution of the Lode angle parameter becomes more complex, and the stress triaxiality is not significantly affected. For circle notched specimen, as the relative notch size increases, there are no significant changes in the stress triaxiality and Lode angle parameter.

(5) There are apparent differences in stress states for SPT specimens with different notch types. When using notched SPT specimen to study mechanical properties, it is necessary to understand the stress state of the studied SPT specimens. Due to the engineering practice, the typical ductile material CuCrZr is considered in this work, and the results of Table 6 and Fig. 31 are limited to ductile materials.

## 6 Conclusion

This study explores the influences of notch type and size on load-displacement curve, fracture energy, strain distribution, failure mode, and stress state of notched SPT specimens, and the stress state characterizations of notched SPT specimens are provided.

(1) Side notch reduces maximum load and membrane stretching slope, and groove notch slightly affects slope but reduces maximum load, while circle notch causes a rapid decrease in load, displacement, and fracture energy.

(2) Side notch shifts strain concentration point from circular ring to notch, with symmetric distribution, and notch size dependent. Groove notch shifts strain concentration point to specimen centre, with "butterfly" shape distribution, and notch size independent. Circle notch converges the strain concentration ring towards the centre point, with asymmetric distribution, and notch size independent.

(3) Side notch affects stress state at the notch location, and stress state on notch arc are highly dependent on notch size. Groove notch affects the stress state on the whole centre line, but the stress state on notch arc is independent on notch size. Circle notch narrows the central biaxial tensile stress area, while the stress state on notch arc is independent on notch size.

(4) Quantitative stress state characterizations are established for notched SPT specimens, vital for mechanical properties and fracture parameter studies by notched SPT specimen.

**Declaration of Competing Interest**

The authors declare that they have no known competing financial interests or personal relationships that could have appeared to influence the work reported in this paper.

**Acknowledgements**

The authors are grateful for the supports provided by the National Natural Science

Foundation of China, grant number 52075050, Natural Science Foundation of Jiangsu Province, grant number BK20201448, Natural Science Foundation of the Jiangsu Higher Education Institutions of China, grant number 23KJA460002. Dr Yiqiang Wang would like to acknowledge the EPSRC grant [EP/W006839/1] for his time.

**Data availability**

Data will be made available on request.

**Reference**

[1] R.C. Hurst, R.J. Lancaster, S.P. Jeffs, M.R. Bache, The contribution of small punch testing towards the development of materials for aero-engine applications, Theor. Appl. Fract. Mech., 86 (2016) 69-77, https://doi.org/10.1016/j.tafmec.2016.07.013.

[2] S. Jeffs, R. Douglas, W. Beard, M. Coleman, J. Adams, T. Jones, D. Poole, R. Lancaster, Characterising the high temperature tensile behaviour of laser powder bed fused duplex stainless steel 2205 using the small punch test, Mater. Charact., 189 (2022) 111953, https://doi.org/10.1016/j.matchar.2022.111953.

[3] J. Zhong, M. Song, K. Guan, P. Dymacek, Application of a database in the evaluation of strengths of Cr-Mo steels by means of small punch test, Int. J. Mech. Sci., 166 (2020) 105195, https://doi.org/10.1016/j.ijmecsci.2019.105195.

[4] W. Sun, M. Li, Z.-X. Wen, G.-Y. Zhou, Z.-F. Yue, S.-T. Tu, Uncertainties in and recommendations to small punch tensile and creep tests for ductile materials, Eng. Fract. Mech., 289 (2023) 109443, https://doi.org/10.1016/j.engfracmech.2023.109443.

[5] W. Sun, S. Li, G.-Y. Zhou, M. Li, Z.-X. Wen, Z.-F. Yue, S.-T. Tu, Interpretation of non-conventional miniaturized creep test: derivation of equivalent gauge length, J. Mater. Res. Technol., 24 (2023) 4390-4404, https://doi.org/10.1016/j.jmrt.2023.04.066.

[6] L. Zhao, X. Wang, L. Xu, Y. Han, H. Jing, Fatigue performance of Hastelloy X at elevated temperature via small punch fatigue test, Theor. Appl. Fract. Mech., 116 (2021) 103118, https://doi.org/10.1016/j.tafmec.2021.103118.

[7] R.V. Prakash, P. Dhaka, G.V. Prasad Reddy, R. Sandhya, Understanding the fatigue response of small volume specimens through novel fatigue test methods – Experimental results and numerical simulation, Theor. Appl. Fract. Mech., 103 (2019) 102304, https://doi.org/10.1016/j.tafmec.2019.102304.

[8] E. Altstadt, F. Bergner, A. Das, M. Houska, Effect of anisotropic microstructure of ODS steels on small punch test results, Theor. Appl. Fract. Mech., 100 (2019) 191-199, https://doi.org/10.1016/j.tafmec.2019.01.014.

[9] W. Wen, G.A. Jackson, H. Li, W. Sun, An experimental and numerical study of a CoNiCrAlY coating using miniature specimen testing techniques, Int. J. Mech. Sci., 157-158 (2019) 348-356,

https://doi.org/10.1016/j.ijmecsci.2019.04.001.
[10] M.D. Callaghan, W.Y. Yeung, M.I. Ripley, D.G. Carr, An Analysis of Deformation and Fracture Behaviour of Zircaloy-4 Alloy Using Small Punch Test, Mater. Sci. Forum, 475-479 (2005) 1415-1420,
https://doi.org/10.4028/www.scientific.net/MSF.475-479.1415.
[11] Y.-S. Chang, J.-M. Kim, J.-B. Choi, Y.-J. Kim, M.-C. Kim, B.-S. Lee, Derivation of ductile fracture resistance by use of small punch specimens, Eng. Fract. Mech., 75 (2008) 3413-3427,
https://doi.org/10.1016/j.engfracmech.2007.06.006.
[12] P. Kubík, F. Šebek, J. Petruška, J. Hůlka, N. Park, H. Huh, Comparative investigation of ductile fracture with 316L austenitic stainless steel in small punch tests: Experiments and simulations, Theor. Appl. Fract. Mech., 98 (2018) 186-198,
https://doi.org/10.1016/j.tafmec.2018.10.005.
[13] I.I. Cuesta, C. Rodriquez, F.J. Belzunce, J.M. Alegre, Analysis of different techniques for obtaining pre-cracked/notched small punch test specimens, Eng. Fail. Anal., 18 (2011) 2282-2287,
https://doi.org/10.1016/j.engfailanal.2011.08.004.
[14] K. Turba, B. Gülçimen, Y.Z. Li, D. Blagoeva, P. Hähner, R.C. Hurst, Introduction of a new notched specimen geometry to determine fracture properties by small punch testing, Eng. Fract. Mech., 78 (2011) 2826-2833,
https://doi.org/10.1016/j.engfracmech.2011.08.014.
[15] Y. Xu, K. Guan, Evaluation of fracture toughness by notched small punch tests with Weibull stress method, Mater. Des., 51 (2013) 605-611,
https://doi.org/10.1016/j.matdes.2013.04.071.
[16] T.D. Shikalgar, B.K. Dutta, J. Chattopadhyay, Assessment of fracture resistance data using p-SPT specimens, Theor. Appl. Fract. Mech., 98 (2018) 167-177,
https://doi.org/10.1016/j.tafmec.2018.10.003.
[17] J.M. Alegre, R. Lacalle, I.I. Cuesta, J.A. Álvarez, Different methodologies to obtain the fracture properties of metallic materials using pre-notched small punch test specimens, Theor. Appl. Fract. Mech, 86 (2016) 11-18,
https://doi.org/10.1016/j.tafmec.2016.09.006.
[18] H.S. Lai, X. Jiang, Determination of fracture toughness through small punch test of notched-tube specimen, Eng. Fract. Mech., 279 (2023) 109059,
https://doi.org/10.1016/j.engfracmech.2023.109059.
[19] I.I. Cuesta, J.M. Alegre, T.E. García, C. Rodríguez, Influence of the notch shape of pre-notched small punch specimens on the creep failure time, Eng. Fail. Anal., 56 (2015) 332-337,
https://doi.org/10.1016/j.engfailanal.2015.01.008.
[20] P. Dymáček, F. Dobeš, D. Andrés, Notch sensitivity of Sanicro 25 in small punch creep test, Theor. Appl. Fract. Mech., 100 (2019) 383-389,
https://doi.org/10.1016/j.tafmec.2019.02.003.
[21] J.M. Alegre, I.I. Cuesta, C. Rodriguez, F.J. Belzunce, Determination of the creep crack initiation properties using pre-cracked small punch tests, Theor. Appl. Fract. Mech., 86 (2016) 39-44,

https://doi.org/10.1016/j.tafmec.2016.08.022.
[22] G. Álvarez, C. Rodríguez, F.J. Belzunce, T.E. García, Use of notched small punch test specimens for the determination of fracture properties in structural steels, Theor. Appl. Fract. Mech., 106 (2020) 102442,
https://doi.org/10.1016/j.tafmec.2019.102442.
[23] T.E. García, C. Rodríguez, F.J. Belzunce, I.I. Cuesta, Development of a new methodology for estimating the CTOD of structural steels using the small punch test, Eng. Fail. Anal., 50 (2015) 88-99,
https://doi.org/10.1016/j.engfailanal.2015.01.011.
[24] E. Martínez-Pañeda, T.E. García, C. Rodríguez, Fracture toughness characterization through notched small punch test specimens, Mater. Sci. Eng., A, 657 (2016) 422-430,
https://doi.org/10.1016/j.msea.2016.01.077.
[25] K. Guan, D. Wang, J. Dobrovská, K. Matocha, Evaluation of the ductile-brittle transition temperature of anisotropic materials by small punch test with un-notched and U-notched specimens, Theor. Appl. Fract. Mech., 102 (2019) 98-102,
https://doi.org/10.1016/j.tafmec.2019.04.003.
[26] K. Matocha, O. Dorazil, R. Hurst, The Present SP Tests for Determining the Transition Temperature T(SP) on "U" Notch Disc Specimens, Materials (Basel), 10 (2017) 490,
https://doi.org/10.3390/ma10050490.
[27] W. Wang, J. Zhong, X. Zhang, T. Jiang, K. Guan, Study of estimation of ductile-brittle transition temperature using U-notched small punch test specimens, Theor. Appl. Fract. Mech., 108 (2020) 102627,
https://doi.org/10.1016/j.tafmec.2020.102627.
[28] R. Hurst, Y. Li, K. Turba, Determination of fracture toughness from the small punch test using circular notched specimens, Theor. Appl. Fract. Mech., 103 (2019) 102238,
https://doi.org/10.1016/j.tafmec.2019.102238.
[29] P. Kumar, B.K. Dutta, J. Chattopadhyay, Fracture toughness prediction of reactor grade materials using pre-notched small punch test specimens, J. Nucl. Mater., 495 (2017) 351-362,
https://doi.org/10.1016/j.jnucmat.2017.08.035.
[30] Y.C. Lin, X.-H. Zhu, W.-Y. Dong, H. Yang, Y.-W. Xiao, N. Kotkunde, Effects of deformation parameters and stress triaxiality on the fracture behaviors and microstructural evolution of an Al-Zn-Mg-Cu alloy, J. Alloys Compd., 832 (2020) 154988,
https://doi.org/10.1016/j.jallcom.2020.154988.
[31] B. Kondori, A.A. Benzerga, Effect of Stress Triaxiality on the Flow and Fracture of Mg Alloy AZ31, Metall. Mater. Trans. A, 45 (2014) 3292-3307,
https://doi.org/10.1007/s11661-014-2211-7.
[32] Z. Li, Y. Zhou, S. Wang, Influence of Strain and Stress Triaxiality on the Fracture Behavior of GB 35CrMo Steel during Hot Tensile Testing, Adv. Mater. Sci. Eng., 2018 (2018) 1-11,

https://doi.org/10.1155/2018/5124524.
[33] A. Srivastava, A. Needleman, Void growth versus void collapse in a creeping single crystal, J. Mech. Phys. Solids, 61 (2013) 1169-1184, https://doi.org/10.1016/j.jmps.2013.01.006.
[34] Y. Zhu, M.D. Engelhardt, R. Kiran, Combined effects of triaxiality, Lode parameter and shear stress on void growth and coalescence, Eng. Fract. Mech., 199 (2018) 410-437, https://doi.org/10.1016/j.engfracmech.2018.06.008.
[35] Y.-S. Ma, D.-Z. Sun, F. Andrieux, K.-S. Zhang, Influences of initial porosity, stress triaxiality and Lode parameter on plastic deformation and ductile fracture, Acta Mech. Solida Sin., 30 (2017) 493-506, https://doi.org/10.1016/j.camss.2017.10.002.
[36] BS EN 10371-2021 British Standards Institution.Metallic materials- Small punch test method., UK, 2021.
[37] BS EN ISO 6892-1: 2019 British Standards Institution. Metallic materials- Tensile testing- Part 1: Method of test at room temperature., UK, 2019.
[38] Y. Zhong, H.S. Lai, J. Guo, P. Du, Q. Huang, Small punch test for investigating circumferential creep in cladding tubes, Int. J. Mech. Sci., 267 (2024) 109001, https://doi.org/10.1016/j.ijmecsci.2024.109001.
[39] K.-W. Seo, Y.-J. Kim, J.-H. Hwang, K.-S. Kim, Finite element simulation method for combined Ductile-Brittle fracture of small punch test in hydrogen, Eng. Fract. Mech., 289 (2023) 109489, https://doi.org/10.1016/j.engfracmech.2023.109489.
[40] K.-H. Kim, Y.-C. Kim, E.-c. Jeon, D. Kwon, Evaluation of indentation tensile properties of Ti alloys by considering plastic constraint effect, Mater. Sci. Eng., A, 528 (2011) 5259-5263, https://doi.org/10.1016/j.msea.2011.03.052.
[41] Z. Liu, X. Wang, Z. Zhang, P. Jin, X. Chen, Solutions and applications of 3D elastic–plastic constraint parameters for clamped single edge notched tension (SENT) specimens, Eng. Fract. Mech., 272 (2022) 108713, https://doi.org/10.1016/j.engfracmech.2022.108713.
[42] N. Bonora, G. Testa, Plasticity damage self-consistent model incorporating stress triaxiality and shear controlled fracture mechanisms – Model verification and validation, Eng. Fract. Mech., 271 (2022) 108635, https://doi.org/10.1016/j.engfracmech.2022.108635.
[43] Y. Bai, T. Wierzbicki, A new model of metal plasticity and fracture with pressure and Lode dependence, Int. J. Plast., 24 (2008) 1071-1096, https://doi.org/10.1016/j.ijplas.2007.09.004.
[44] T. Wierzbicki, L. Xue, On the effect of the third invariant of the stress deviator on ductile fracture. Technical report, Impact and Crashworthiness Laboratory, Massachusetts Institute of Technology, Cambridge, MA, USA, 2005.